UNEP IMEO Technical Documentation for Methane Satellite Detection and Quantification

1. Introduction

UNEP's International Methane Emissions Observatory (IMEO) launched the Methane Alert and Response System (MARS) in a pilot phase at COP-27 and a fully-operational phase at COP-28. MARS increases transparency and accelerates implementation of the Global Methane Pledge (GMP) by bringing together four critical components: (1) satellite detection of large sources of anthropogenic methane emissions, (2) notification of relevant stakeholders about these detected emissions, (3) assessment and mitigation of emission events and (4) tracking and documentation of events, including public sharing of data.

Building a comprehensive understanding of where methane emissions come from and how those emissions change over time is widely considered critical to realize deep reductions in methane emissions. UNEP IMEO is leveraging the state of the art of current remote sensing technologies to detect and localize very large point source emissions from human activity (energy, waste, agriculture). The rapid expansion of satellite capability is increasingly allowing for the detection of lower and lower emissions rates at increased frequency and detection of area source emissions (e.g., from oil and gas, agriculture).

This document provides an overview of the scientific principles and methodologies employed by UNEP IMEO and its partner organizations to use satellites to *detect* and *quantify* methane point source emissions from satellites. While this document is not comprehensive in its descriptions, additional information can be found in the published scientific literature citations found throughout this document. UNEP IMEO satellite (and other) methane data is published via the UNEP IMEO Eye on Methane portal.

2. Basic Scientific Principles

The general principles of methane detection and quantification from satellites can be found in Jacob *et al.*, (2016; 2022). Below we summarize the main points from these works.

Methane detection from space relies on the basic principles of imaging spectroscopy. Atmospheric methane is detectable because it absorbs radiation in the shortwave infrared (SWIR) at 1.65 and 2.3 μm, and in the thermal infrared (TIR) at 8 μm. **Figure 1** from *Jacob et al., (2016)* shows the atmospheric optical depths (AOD) of different trace gasses in the atmosphere. Both SWIR channels are used for satellite remote sensing because the methane signal can be unambiguously determined because other atmospheric trace gasses do not obscure the absorption spectra. Because TIR measurements are mostly sensitive to methane in the upper atmosphere, they are less effective for detecting and quantifying methane emissions that occur at the Earth's surface since thermal radiation is more prominently emitted by gasses at higher altitudes.

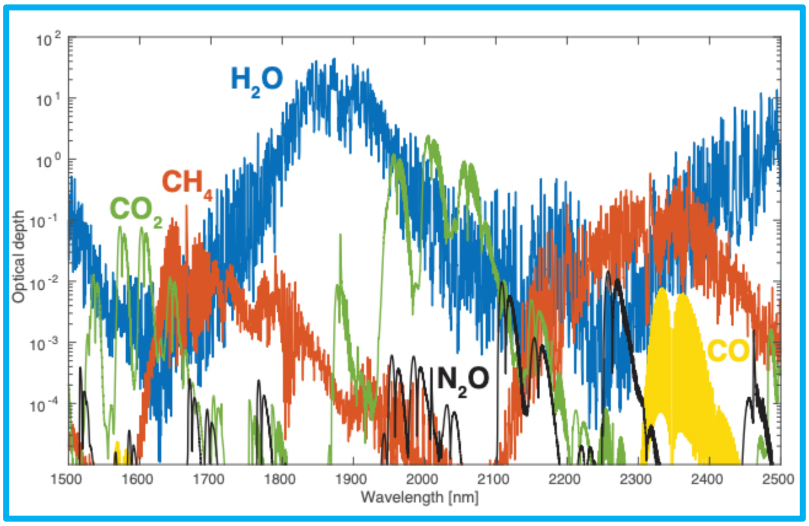

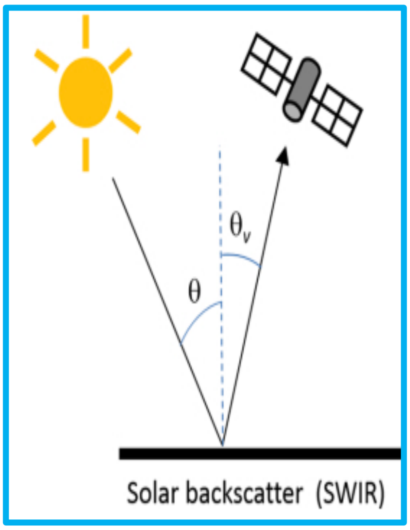

Figure 1: Atmospheric optical depth (AOD) of major trace gasses for the US Standard atmosphere showing methane detection channels in the SWIR (Figure 4 from *Jacob et al., 2016*)

Figure 2: Configuration of passive SWIR satellites (q and qv are solar zenith and satellite viewing angles; from *Jacob et al., 2019* Figure 2)

Most methane-detecting satellites are *passive* – they rely on reflected sunlight from the surface to provide a signal (**Figure 2**). To retrieve methane at either SWIR channel, the reflected solar spectrum measured by the satellite instrument is fit to a modeled spectrum, normalized by the geometric air mass factor, and the total vertical column density of methane is determined (Ω; molecules cm^{-2}). Note that the measured slant column density is normalized by the geometric air mass factor ($cos^{-1}\theta + cos^{-1}\theta_v$; where θ and θ_v are the solar and satellite viewing angels, respectively) to account for the viewing geometry of the satellite. Finally, to remove the sensitivity of the vertical column density to surface pressure changes, it is converted to a dry air column-average mole fraction or column-average mixing ratio ($X_{CH4} = \Omega/\Omega_a$ where Ω_a is the vertical column density of dry air from the local pressure and humidity).

Because methane-detecting satellite instruments rely on reflected sunlight for their signal, they have some innate detection limitations. First, the presence of clouds inhibits sunlight reflection from the surface, making near-surface methane undetectable in cloudy pixels. Nighttime observations are not possible, and high-latitude observations are difficult during low-sunlight conditions due to the lack of reflected solar signal. Dark surfaces, such as over water or in densely forested regions, absorb incoming solar radiation and reduce the signal reflected back to the satellite, making detection more difficult, but not impossible depending on specific sensor characteristics and sun angle. Heterogenous surfaces, such as in mountainous regions or in cities, and snowy surfaces can also increase the difficulty for methane retrieval.

3. Methane-Detecting Satellite Characteristics

Most methane-detecting satellites are generally **Low Earth Orbit** (LEO; altitude of 2000 km or less) and **sun-synchronous** (passes over each area of the world at approximately the same solar local time of day) to maximize the signal of reflected sunlight. These types of satellites revolve around the Earth, imaging along a **swath** (area imaged on surface). They also have **revisit periods** – the time it takes for the satellite to return and reimage the same location on the Earth – which is a function of both the satellite orbit and its ability to target or not (see below). There is now the capability to also use some **geostationary** weather satellites (*Watine-Guiu et al.,* 2023) to detect very, very large methane emissions; these types of satellites are at such a high altitude that they orbit the Earth at its rotation speed, thus continuously imaging a portion of the Earth's surface (e.g., over the Americas). More general information on satellites and remote sensing is available from the Canada Center for Mapping and Earth Observation, Natural Resources Canada.

Methane can be detected from either ***area sources*** or ***point sources***. Area sources can be both *diffuse* (e.g., emissions from wetlands over the area of the wetland) or can represent the integral of a very large number of individually small emitters (e.g., cumulative emissions from low-production oil wells; *Omara et al.,* 2022). Point sources represent emissions, for example, from a single facility or piece of equipment within a facility, (*Duren et al.,* 2019).

Following [Jacob et al., (2022)](), methane-detecting satellites can be classified in terms of their ability to observe methane on global- and regional-scales, as well as by their capability to determine emissions from area sources or on the scale of individual point sources. **Figure 4**, adapted from Jacob et al., (2022), describes these classifications pictorially.

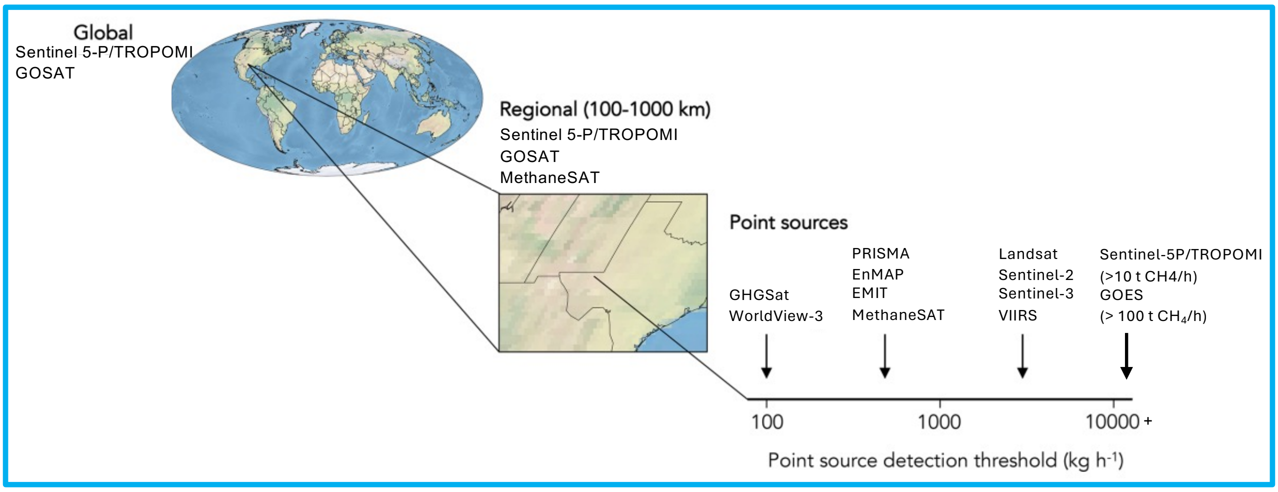

Figure 4: Satellite classification for global mapping, area flux (regional) and point source imaging satellites. Point source detection thresholds (i.e., Minimum Detection Limits (MDL) in ideal observing conditions) are shown by order of magnitude. Figure adapted from *Jacob et al.*, 2022 their Figure 4).

Global mapping satellites – such as the European Space Agency's (ESA) Sentinel-5P/TROPOMI satellite – typically have lower spatial-resolution pixels but very frequent revisit periods and frequent global coverage thanks to a wide swath, and a high sensitivity for detecting methane. These types of satellites can be used for global-to-regional emissions using **inverse flux inversion methods** (*Jacob et al.*, 2022). Averaging the X_{CH4} retrievals from these instruments, including utilizing wind-rotation techniques, is useful for locating **'hot-spots'**, or regions of enhanced methane concentration resulting from one or more persistent emissions sources (Maasakkers *et al.*, 2022). Additionally, these satellites can detect very large (> 10 tonnes methane per hour) point source emissions (e.g., *Lauvaux et al.*, 2022). UNEP IMEO uses these types of instruments for both use cases – determining **Regions of Interest** (ROI) to explore with high-resolution point source imagers and for finding very large point source emission plumes.

Point source imagers typically have very high spatial resolution with pixels of 60 m or less. Because of this characteristic, methane emissions plumes obtained from these instruments are attributable at the facility-scale. These types of instruments can either take data *continuously* or be *tasked* (*targeted*). Because of their resolution and narrow swath width, *continuously* viewing point source imagers can only view the same location on the Earth after several days. *Targeted* or *tasked* satellites view limited locations provided by end users.

Between **point source imagers** and **global mapping satellites** are **area flux mappers**, such as MethaneSAT from the Environmental Defense Fund (EDF) and New Zealand Space Agency's. These instruments have higher spatial resolution than global mappers, but similarly high sensitivity to methane. However, they typically take data over limited regions of the Earth, such as only over major oil and gas producing basins. These instruments can determine emissions from both *area* and *point sources,* providing a more complete picture of total methane emissions at regional and sub-regional scale.

UNEP IMEO uses this existing suite of Earth Observation satellites (**Figure 5**) to detect, localize, and quantify large human emission sources globally. Data from these satellites is publicly available, though in some cases specialized remote sensing expertise is required to properly interpret these data. UNEP provides this expertise to the global community to help further the goals of the Global Methane Pledge. Figure 5 and **Table 1**, adapted from *Jacob et al., (2022)*, provide information on satellites with publicly available data useful for detecting methane.

Figure 5: Methane-sensing satellites used by UNEP IMEO, or planed to incorporate in the future. Information on future satellites and commercial satellites is available through the CEOS GHG Satellite Missions Portal.

Additional information on methane-sensing satellites, including from the private sector and not-yet launched, can be found on the Greenhouse Gas Satellite Missions portal from the Committee on Earth Observation Satellites (CEOS).

4. Retrieval Methodologies

Currently, as many of the satellites capable of detecting methane were not, in fact, designed for this purpose, methane enhancement data is not available from space agencies and requires expertise provided by UNEP IMEO to derive these data from radiance data. Here we describe, briefly, methodologies for retrieving methane enhancements from the satellites used by UNEP IMEO. These methodologies vary depending on the instrument type. The vast majority of plumes published on the Eye on Methane platform are processed in-house by the MARS data team. This includes data from high-resolution multispectral (Sentinel-2, Landsat-8/9) and hyperspectral (EMIT, PRISMA, EnMAP) satellites, which together account for the bulk of the detections. MARS also processes geostationary data (GOES) in-house, though these detections are extremely rare. Conversely, detections from global low resolution mapping satellites, specifically TROPOMI (emission hot-spots and plumes), and VIIRS and Sentinel-3 SLSTR point source detections, are processed by our partner organization, the Netherlands Institute for Space Research (SRON), with TROPOMI plume level data enabled by the Copernicus Atmosphere Monitoring Service (CAMS).

TROPOMI Hot-Spots. The European Space Agency (ESA) provides an operational X_{CH4} data product using a full-physics retrieval detailed in *Hasekamp et al.,* (2022). To this product, the Netherlands Institute for Space Research (SRON) has developed regularization and posteriori correction schemes based on TROPOMI X_{CH4} data to reduce biases in the data due to, for example, surface albedo (*Lorente et al.*, 2021). This corrected data product forms the basis for the determination of **'hot-spots'** – locations with persistently enhanced methane concentrations based on long-term averages of TROPOMI X_{CH4} data (*Maasakkers et al.,* 2022). A wind-rotation technique, in which for a target point, data is rotated on individual days based on the wind direction at 10 m such that the wind vector always aligns north, allows localization of methane sources when the downwind concentration is consistently enhanced compared to the upwind concentration. UNEP IMEO uses TROPOMI hot-spots to direct *targeting* and *monitoring* of locations of high-probability methane emissions with high-spatial resolution satellites (*Irakulis-Loitxate et al., 2022*). **Appendix A** provides additional details on the hot spot data provided by SRON.

VIIRS and Sentinel-3 SLSTR Short-lived Ultra-emitters. Short-lived ultra-emitter methane events are detected and quantified by SRON using thermal infrared observations from the VIIRS and SLSTR instruments aboard the Joint Polar Satellite System (JPSS) constellation and Sentinel-3 satellites, respectively (*de Jong et al., 2025*). The JPSS constellation includes NOAA-20 (JPSS-1) and NOAA-21 (JPSS-2), operated by the U.S. National Oceanic and Atmospheric Administration (NOAA), with a typical equatorial overpass near 13:30 local time and a spatial resolution of 750 m. Sentinel-3, operated by the European Space Agency (ESA), provides SLSTR data at a nominal spatial resolution of 500 m with a revisit frequency of under two days. Methane total column enhancements are retrieved using an adapted Multi-Band Multi-Pass (MBMP) method (*Varon et. al., 2021*). The observed reflectance ratios are compared against radiative transfer simulations to quantify the methane enhancement. Anomaly detection is performed using a robust statistical approach based on the Median Absolute Deviation (MAD) to identify significant deviations from background levels. Emission quantification is carried out by converting the enhancement signal into methane mass under standard pressure assumptions and summing the mass within a spatial mask encompassing the detected plume.

Table 1: Current Methane-Detecting instruments used by UNEP IMEO

Type[a]	Agency[b]	Satellite System	Number of Satellites	Launch Year	Pixel Resolution [km]	~Detection Limit (MDL)[c] [CH_4 t/h]	~ Return Time [days][d]	Tasking[e]	Purpose[f]
Global Mapper	ESA	Sentinel-5P/TROPOMI[g]	1	2017	7 × 5.5	10	1	N	Archive
	JAXA, MOE, NIES	GOSAT[h]	1	2009	10 (diameter; circular pixels)	10	3	N	Archive
Geostationary	ESA, EUMESAT	Meteosat Third Generation	1	2022	~1 × 1	30	10 minutes	N	Notification
	NOAA	GOES[i]	2	2016	~2 × 2	100	5-10 minutes	N	Notification
Area Mapper	EDF	MethaneSAT	1	2024	0.20 × 0.40	2-3	3-4	Y	Notification
Point-Source Imager	ESA	Sentinel-2	3	2015	0.02 × 0.02	1	2-5	N	Notification
	ESA	Sentinel-3	2	2016	0.50 × 0.50	10	1	N	Notification
	NOAA, NASA	VIIRS	3	2011	0.75 × 0.75	10	< 1	N	Notification

	NASA, USGS	Landsat-4/5/7	3	1982	0.03 × 0.03	1	16	N	Archive
	NASA, USGS	Landsat-8/9	2	2013	0.03 × 0.03	1	16	N	Notification
	ASI	PRISMA	1	2019	0.03 × 0.03	0.5	4	Y	Notification
	DLR	EnMAP	1	2022	0.03 × 0.03	0.5	4	Y	Notification
	CNSA	GaoFen-5	2	2018	0.03 × 0.03	0.5	5	Y	Notification
	NASA	EMIT[j]	1	2022	0.06 × 0.06	0.3	3	N	Notification
	GHGSat	GHGSat	15	2016	0.02 × 0.02	0.1	1-2	N	Archive
	Carbon Mapper	Tanager-1	1	2025	0.03 × 0.03	0.1	1-7	N	Notification
	EDF	MethaneAIR[k]	1	2024	0.005 × 0.025	0.1	On campaigns	N	Notification

[a]Classification as **Global Mapper** (near-daily global coverage, lower-spatial resolution, high precision), **Area Mapper** (medium-spatial resolution, high-precision instrument for area emissions and point source emissions), **Point Source Imagers** (high-resolution with pixel size on order of 60 m or less; useful for localization of emissions to facility scale; can be *targeted* or *continuously monitoring*), and **Geostationary** (very high-frequency, low-spatial resolution observations over a region of globe; can quantify total event emissions and not just instantaneous emission rate).

[b]JAXA = Japan Aerospace Exploration Agency, MOE = Ministry of Environment, NIES = National Institute for Environmental Studies, ESA = European Space Agency, NASA = National Aeronautics and Space Administration, DLR = Deutsches Zentrum für Luft-und Raumfahrt, USGS = United States Geological Survey, ASI = Agenzia Spaziale Italiana, NOAA = National Oceanic and Atmospheric Administration, CNSA = China National Space Administration

[c]**Minimum Detection Limit (MDL)** is level below which satellite is unable to detect emissions from point sources; note that inability to detect does not necessarily indicate that emissions don't exist, as they may be below the MDL. MDLs are a function of sensor characteristics *and* environmental/observing conditions. Generally, they are provided for the best observing conditions (homogenous, bright, dry surface with no vegetation, no clouds, and moderate wind). Further from these ideal conditions, the detection limit will be higher.

[d]Time interval between successive viewings of the same scene/location on Earth's surface.

[e]Targeted or tasked instruments take data over provided locations, rather than continuously everywhere along orbit.

[f]**Purpose** denotes the primary application of the observations. *Notification* supports the rapid detection and reporting of recent super-emitter events, whereas *Archive* supports the development of historical records and time-series analyses.

[g]Sentinel-5P is used by UNEP IMEO both to provide methane **'hot-spots'** (regions of elevated methane concentration) for high-resolution satellite targeting, and for providing large (> 10 tonnes CH_4 per hour) methane plume (point source) emissions data.

[h]GOSAT data is low-resolution and used to provide 'hot-spot' data for high-resolution satellite targeting.

[i]GOES is a **geostationary** satellite providing near-continuous observations over the Americas; it is used to monitor very, very large (> 100 tonnes CH_4 per hour) emissions events and to target high-resolution satellites. Resolution is 1 km × 1 km to 2 km × 2 km. Because it takes data nearly-continuously, event integrated emissions can be determined.

[j]EMIT is an instrument aboard the International Space Station (ISS). It has coverage between +51.6°N and 51.6°S.

[k]Aerial instrument used in targeted observation campaigns and to supplement observations following the loss of MethaneSAT.

TROPOMI Methane Point Sources. CAMS TROPOMI's methane point source plumes, processed by SRON, use the operational Level 2 Copernicus Sentinel-5P TROPOMI X_{CH4} data from ESA following

Schuit et al., (2023). The TROPOMI instrument provides daily global coverage of methane concentrations at up to 7 x 5.5 km^2 spatial resolution. These observations enable the detection of very large methane plumes worldwide. However, TROPOMI plumes have a localization error of approximately ±50 km, so these plumes themselves are not attributable to facility-scale unless plumes are either in regions with sparse potential emissions sources or are coincidentally viewed with other high-resolution satellites, particularly those with nearly contemporaneous overpass times (e.g., Sentinel 3 *Pandey et al.*, 2023; VIIRS *de Jong, et al.*, 2024). The plumes are provided here on a weekly basis through CAMS. **Appendix B** provides further details on the methodology used by SRON to derive methane point source plumes from TROPOMI data.

High-resolution hyperspectral satellites. Satellites such as PRISMA, EnMAP, EMIT, Tanager-1, or GaoFen-5 combine high spatial resolution (30 m × 30 m to 60 m × 60 m) and high spectral resolution (e.g., < 5 nm spacing between spectral lines). They feature numerous spectral channels keyed to methane's strong methane absorption features around 2.3 µm. Methane retrievals from these satellites are computed using both a standard **Match-Filter (MF)** and a **Wide-Window Match-Filter (WWMF)** approach (Roger *et al.,* 2024), as detailed in numerous scientific papers (PRISMA *Guanter et al.,* 2021; EnMAP Roger et al., 2023, 2024; GaoFen-5 *Irakulis-Loitxate et. al.*, 2021; Tanager-1 *Duren et. al., 2025*), involves detecting methane's absorption spectrum using statistics extracted from the hyperspectral image. Radiative transfer simulations are subsequently utilized to derive per pixel methane concentration enhancements. While EnMAP and PRISMA are sometimes tasked for specific locations of interest, all data from these three sensors is automatically ingested and pre-processed and plumes are initially flagged using the AI model described in Růžička et al. (2025). UNEP IMEO applies the MF and WWMF retrieval methods to derive methane from L1B satellite radiance data provided by the respective space agencies. **Appendix C** provides additional data on the MF and WWMF methodologies for methane retrievals from hyperspectral data.

High-resolution multispectral satellites. Satellites such as Sentinel-2, Landsat-8, Sentinel-3 or GOES, offer frequent and extensive observations across vast regions, albeit with a lower sensitivity to methane due to their lower spectral resolution. Under certain favorable observation conditions, such as strong emissions and background homogeneity, methane retrievals can be performed using the **Multi-Band-Multi-Pass (MBMP)** approach. This method, as detailed in studies by *Varon et. al.* (2021), *Irakulis-Loitxate et al.*, (2022a,b); *Pandey et. al.* (2023), *Gorroño et al.*, (2023) and *Watine-Guiu* *et. al.* (2023), leverages the varying levels of absorption in various shortwave infrared spectrum bands when methane is in the satellite's line of sight. Radiative transfer simulations are similarly employed to derive per pixel methane concentrations (X_{CH4}). UNEP IMEO applies the MBMP retrieval method to derive methane from L1B or L1C satellite radiance data provided by the respective space agencies. For Sentinel-2 and Landsat 8/9, this data is automatically ingested and potential plumes are flagged by the MARS-S2L AI model (Allen et al., 2025) **Appendix D** provides additional details on the MBMP methodology for multispectral satellites.

5. Plume Masking and Emissions Estimation

Quantification of methane emissions from a single satellite observation center on the instantaneous source rate (*Q*; mass methane emitted per time unit), which reflects the emission rate at the time of observation. Emissions from a point source produce a turbulent 'plume' which shape and extent depend on the emissions source strength, the wind, and atmospheric turbulence (a function of atmospheric stability and surface roughness; *Varon et al.*, 2018). **Figure 6** from *Guanter et al., (2024)*. shows some examples of methane plumes from lower- and higher-spatial resolution methane-detecting satellites (i.e., global mapping versus point source imager).

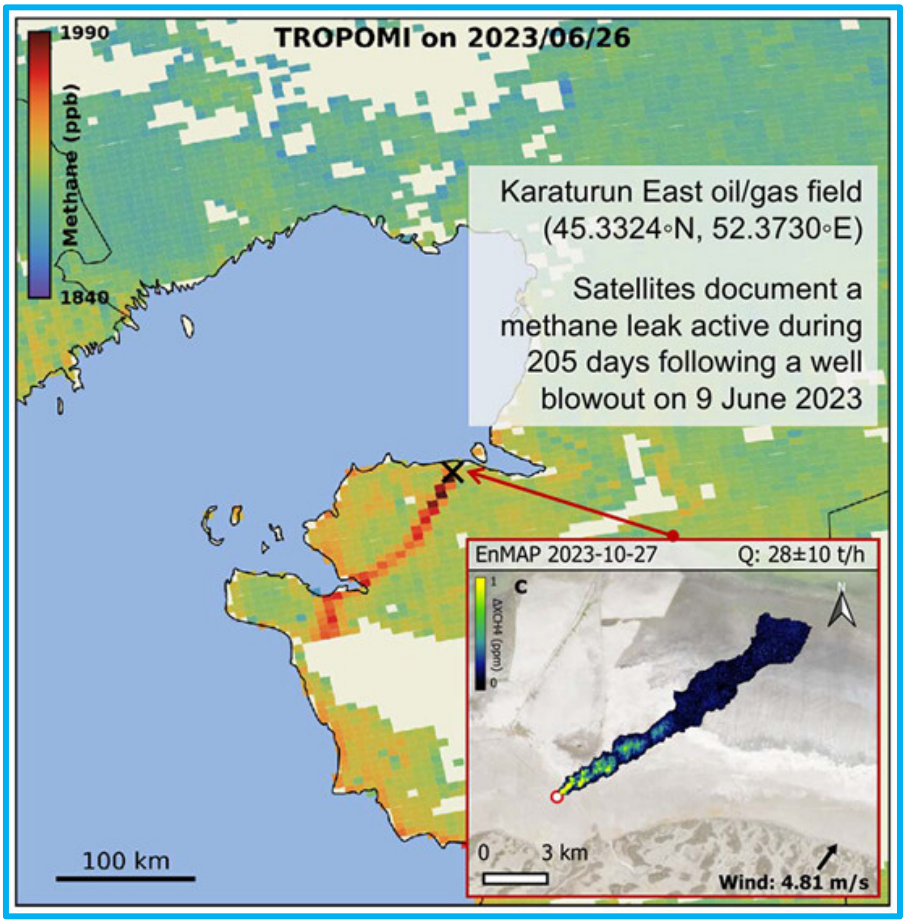

Figure 6: Methane plumes from Sentine-5P/TROPOMI (lower-spatial resolution global mapping satellite) and EnMap (DLR's high-spatial resolution point source imager). Figure from *Guanter et al., 2024*.

Before estimating plume emission rates, for many quantification methodologies a **plume 'mask'** must be determined. The plume mask represents the physical extent of the plume, and it is determined through pixel selection procedures that separate the signal of methane enhancement from noise. Statistical algorithms, machine learning algorithms (Allen *et al.,* 2025; Růžička *et al.,* 2025), and human evaluation can be used to construct such masks that consider only the pixels with significant signal-to-noise ratios within a scene to be part of a methane plume. **Appendix G** provides details on the plume-masking methods utilized by UNEP IMEO.

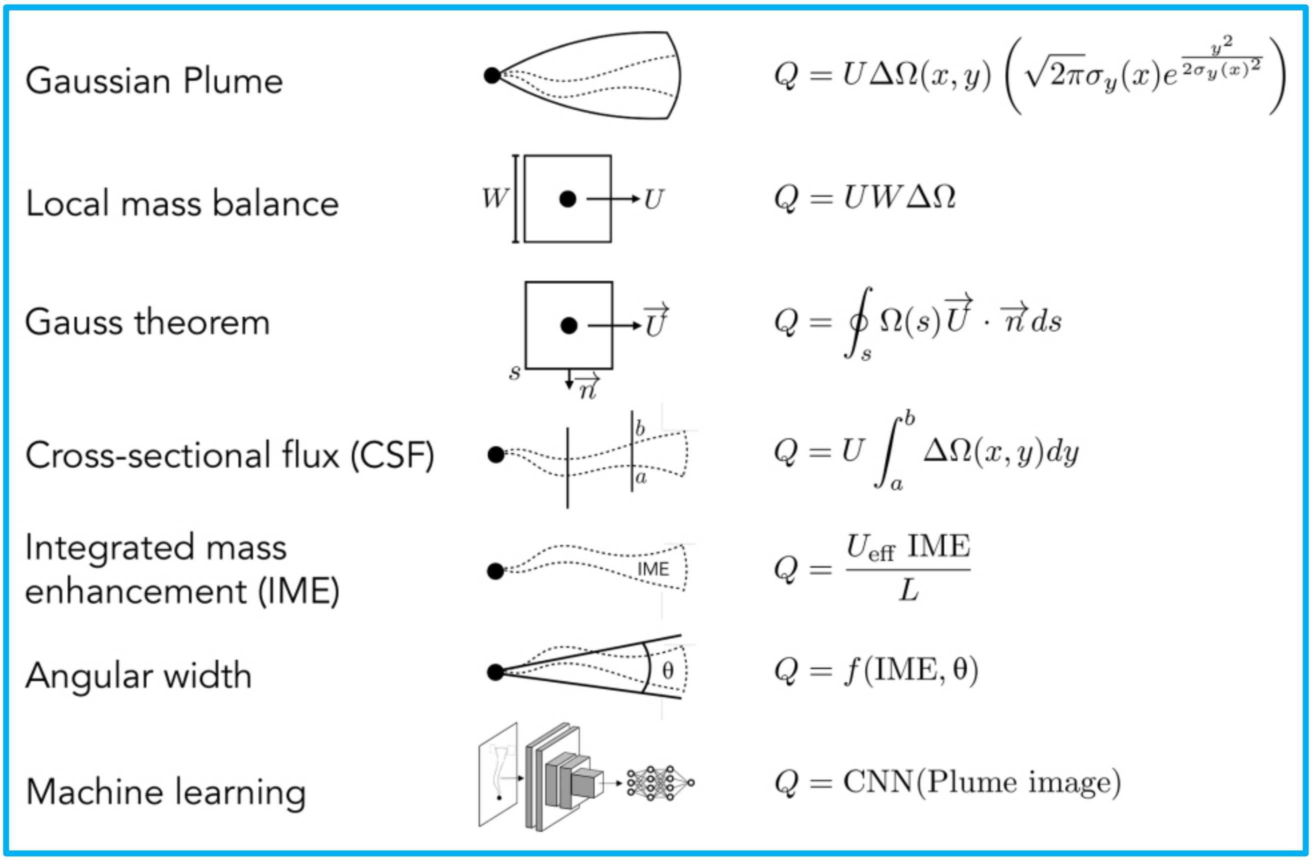

Figure 7: Pictorial representation of methods used to quantify point source emission rates (Q; mass per unit time) from point source imagers. UNEP IMEO uses the IME method described below. Figure from *Jacob et al., (2022*; their Figure 6) with additional details on other methodologies available in that reference.

Multiple-methodologies can be used to infer point-source emission rates (*Q*) from satellite data. **Figure 7** from *Jacob et al., (2022)* illustrates these methods and more details on each can be found in that reference. UNEP IMEO utilizes the **Integrated Mass Enhancement (IME)** method, which calculates the total mass of methane by integrating the concentration enhancements detected in each pixel over the entire area of the observed plume. To determine the source rate, an empirical linear relationship is applied, incorporating the effective wind speed and the length of the plume, as described by *Frankenberg et. al. (2016)*:

$$Q = \frac{U_{eff} \cdot IME}{L}$$

where Q is the point source emission rate [kg s^{-1}], U_{eff} [m s^{-1}] is the effective wind speed – itself a function of the 10 m wind speed and surface turbulence characteristics, and L [m] is the horizontal extent of the plume. Additional details on the IME algorithm are found in *Varon et al., (2018).* **Appendix G** provides more details on the IME methodology employed by UNEP IMEO.

6. Emissions Uncertainties and Validation

Plume misidentification errors: False positives occur when a methane plume seems to exist when no plume exists. This can occur, for example, when reflection from a surface feature appears as a plume-like structure in the satellite reflectance data. **False negatives** occur when a plume exists but is not detected. Both types of errors are more likely when plume detection and masking is performed solely using computer algorithms (statistical or AI-enhanced). False negatives can also occur when the emission flux rate is at the edge of the detection limit of the satellites, and there is insufficient confidence to determine if the observed enhancement is an emission without additional information. At UNEP IMEO, while some deep-learning models are used to initially detect plumes (Allen *et al.*, 2025; Růžička *et al.*, 2025) trained expert analysts *always* provide quality control on *every* plume published to avoid these types of errors. **Appendix F** details UNEP IMEO's quality control approach to avoid false positive plumes.

Quantification errors: Sources of error for quantification include the extent of the plume (L), which depends on the plume mask determination, and, more importantly, the effective wind speed U_{eff}. Low wind speeds make emissions estimation challenging because, though they improve signal-to-noise, the plume length (L) determination is difficult. Conversely, conditions with very high wind speeds are difficult because quicker dispersion potentially makes the plume more difficult to be detected over the background. Because measured wind data is generally not available locally, the 10-m wind speed (U_{10}) from reanalysis data is generally used. These operational data, provided by meteorological and space institutions such as the European Center for Midrange Weather Forecasting or the NASA Global Modeling and Assimilation Office, introduce representational error because they are only available at lower resolution (e.g., 10- or 25-km grids). This representation error ranges between 15 to 50% depending on satellite sensor precision and environmental conditions (wind speed) at the time of observation (*Varon et al.* 2018). This uncertainty is reflected in the uncertainty estimate for every emission rate provided. **Appendix G** provides details on UNEP IMEO's estimation methods for uncertainty quantification.

Validation: Quantification methodologies, as applied to the date from satellites in use by UNEP IMEO, have been validated by single-blind controlled release studies (*Sherwin et al., 2024*, *2023*). In these studies, methane is released with a metered rate at a known location and time. Multiple teams of experts applied various quantification methodologies to satellites including Sentinel-2, Landsat, PRISMA, EnMAP, and GaoFen-5 to estimate emissions from these sites without knowing the actual metered rate, if methane was released or not, and with and then without knowledge of local wind speeds. Overall, satellites were found to perform similarly to aircraft in terms of quantification error (i.e., within ±50% of the metered value). Minimum detection limits are 1 to 3 orders of magnitude higher than aircraft due to the significantly greater distance of satellites to the emission source. However, the controlled released studies thus far have taken place in regions with high-quality observing conditions (desert region with low cloud cover, high surface albedo, low surface heterogeneity, remote from other potential emission sources, and favorable wind conditions). In those conditions, satellite performance is expected to be at its highest, with commensurately low Minimum Detection Limits (MDL). Future studies, sponsored by UNEP IMEO, will extend these controlled release studies to account for variable observing conditions to better test satellite performance in less-than-ideal cases, and to test a wider range of metered release rates. To compensate for the lack of controlled release experiments in other scenarios and in different observing conditions, satellite measurements are also validated and recalibrated using simulations with synthetic plumes (*Gorroño et al.,* 2023).

7. Source-level statistics

Persistency: Persistency is an estimate of how often emissions are detected from a specific source over time. It looks at the number of times emissions were detected compared to the number of valid observations (*Ayasse et al., 2024*). A valid observation is a clear-sky image with enough quality to allow the detection of emissions. Observations with clouds, haze, shadows or smoke are discarded through automated and manual labelling, The calculation also ignores observations from instruments with a low Probability of Detection (PoD) for the size of the historically detected emissions. MARS calculates persistency of emissions considering the observations available over the past 180 days. Based on the persistency value, the source is classified as: (1) Absent – emissions have not been detected (only for internal use), (2) Sporadic – detected rarely, up to 20% of the times there is a valid observation, (3) Frequent – detected occasionally, within 20-80% of the times of valid observations, (4) Persistent – detected almost every time, between 80% and 100% of valid observations. If there are few valid observations available (less than 4), the persistency is set to Undetermined. **Appendix J** describes in more detail the methodology behind the computation of persistence.

8. Coal and waste sector

Methane detection in the Coal and Waste sectors relies exclusively on hyperspectral satellite instruments: PRISMA - ASI, EMIT - NASA, and EnMAP - DLR. These sensors provide the spectral resolution needed to detect methane over the complex and heterogeneous surface types typical of coal mines and waste sites, but they cover the Earth less frequently than the multispectral constellation used in Oil & Gas. As a result, fewer plume detections are reported for these sectors, which reflects observational frequency rather than differences in emission levels or persistence.

Source identification in these sectors also follows a different logic than in Oil & Gas. Rather than relying solely on TROPOMI hotspots as a starting point, detection efforts are guided by facility databases, emissions inventories, and national databases such as mining concession registries. This approach allows for the explicit targeting of known installations regardless of whether a prior detection record exists for them. In the case of waste, where emissions tend to be more spatially diffused, this inventory-driven approach is particularly important.

Coal: why coal grade matters

Within the Coal sector, sources are classified by coal grade: thermal coal, metallurgical (met) coal, or thermal & met. Tracking each grade separately serves two distinct purposes.

Thermal coal is used primarily for power generation and is being phased out as part of global climate commitments. Major institutional frameworks, including the UN-convened Net-Zero Asset Owner Alliance, call for the cancellation of new thermal coal projects and a full phase-out of thermal coal power generation. As these assets are progressively retired, tracking thermal coal mine emissions in MARS allows for monitoring how this subsector evolves over time and whether emission reductions align with international commitments.

Metallurgical coal follows a different path. It is used in steel production, and its decarbonization is being tackled through the steel value chain. The Steel Methane Programme (SMP), led by IMEO/UNEP, brings together science, data and industry engagement to make methane emissions from coal and steel visible and actionable, moving from estimated to measured mine-level data. MARS contributes directly to this effort by detecting and tracking met coal methane emissions from space, providing satellite-based measurements.

For further methodological details, please refer to the SMP technical documentation.

Emission sources and attribution

The main emission source types monitored across both coal grades are ventilation systems, degasification (drainage) systems, and other source types associated with mining operations.

Source attribution relies on GEM (Global Energy Monitor), which provides facility-level information including coal grade classification. Through its Coal Mine Boundaries and Methane Sources research, GEM has also mapped mine boundaries and identified potential point sources of emissions across hundreds of mines. This work directly supports MARS attribution efforts, both in linking detections to a specific operating mine and in identifying the type of emission source involved.

Given its spatial resolution, TROPOMI-based detections cannot be confidently attributed to a specific mine or coal grade and are therefore reported with a sector-only label.

7. References

Aybar, C., Ysuhuaylas, L., Loja, J., Gonzales, K., Herrera, F., Bautista, L., Yali, R., Flores, A., Diaz, L., Cuenca, N., Espinoza, W., Prudencio, F., Llactayo, V., Montero, D., Sudmanns, M., Tiede, D., Mateo-García, G., & Gómez-Chova, L. (2022). CloudSEN12, a global dataset for semantic understanding of cloud and cloud shadow in Sentinel-2. Scientific Data, 9(1), Article 1. doi:10.1038/s41597-022-01878-2

Ayasse, A. K., Cusworth, D. H., Howell, K., O'Neill, K., Conrad, B. M., Johnson, M. R., ... & Duren, R. (2024). Probability of Detection and Multi-Sensor Persistence of Methane Emissions from Coincident Airborne and Satellite Observations. Environmental Science & Technology, 58(49), 21536-21544. doi: 10.1021/acs.est.4c06702

Allen, A., Mateo-García, G., Irakulis-Loitxate, I., Montesino-San Martín, M., Watine, M., Requeima, J., Gorroño, J., Randles, C., Mokalled, T., Guanter, L., Turner, R. E., Cifarelli, C., & Caltagirone, M. (2025). Artificial intelligence for methane detection: from continuous monitoring to verified mitigation. arXiv. https://doi.org/10.48550/arXiv.2511.21777

Baudes, A., Coll, B., and Morel, J-M. (2005), A review of image denoising algorithms, with.a new one. *Multiscale Model Simul,* 4, 490-530, doi:10.1137/04061624.

Berk, A., Conforti, P., Kennett, R., Perkins, T., Hawes, F., van den Bosch, J., (2014), Modtran® 6: a major upgrade of the modtran® radiative transfer code. In: 2014 6th Workshop on Hyperspectral Image and Signal Processing: Evolution in Remote Sensing (WHISPERS), pp. 1–4. doi:10.1109/WHISPERS.2014.8077573

Duren, R.M., Thorpe, A.K., Foster, K.T., Rafiq, T., Hopkins, F. M., Yadav, V., Bue, B. D., Thompson, D. R., Conley, S., Colombi, N. K., Frankenberg, C., McCubbin, I., B., Eastwood, M. L., Falk, M., Herner, J. D., Croes, B. E., Green, R. O., and C. E. Miller (2019), California's methane super-emitters. *Nature*, 575, 180–184, doi:10.1038/s41586-019-1720-3.

Duren, R., Cusworth, D., Ayasse, A., Howell, K., Diamond, A., Scarpelli, T., Kim, J., O'neill, K., Lai-Norling, J., Thorpe, A. and Zandbergen, S.R., 2025. The Carbon Mapper emissions monitoring system. *Atmospheric Measurement Techniques*, *18*(22), pp.6933-6958.

Ehret, T., De Truchis, A., Mazzolini, M., Morel, J. M., D'aspremont, A., Lauvaux, T., ... & Facciolo, G. (2022). Global tracking and quantification of oil and gas methane emissions from recurrent sentinel-2 imagery. *Environmental science & technology*, *56*(14), 10517-10529. doi: 10.1021/acs.est.1c08575.

Foote, M.D., Dennison, P.E., Thorpe, A.K., Thompson, D.R., Jongaramrungruang, S., Frankenberg, C., Joshi, S.C., (2020), Fast and accurate retrieval of methane concentration from imaging spectrometer data using sparsity prior. IEEE Trans. Geosci. Remote Sens. 58 (9), 6480–6492, doi:10.1109/TGRS.2020.297688.

Gorroño, J., Varon, D. J., Irakulis-Loitxate, I., and Guanter, L., (2023), Understanding the potential of Sentinel-2 for monitoring methane point emissions, *Atmos. Meas. Tech.*, 16, 89–107, doi.org/10.5194/amt-16-89-2023.

Guanter, L., Irakulis-Loitxate, I., Gorroño, J., Sánchez-García, E., Cusworth, D. H., Varon, D. J., Cogliati, S., and R. Colombo, (2021), Mapping methane point emissions with the PRISMA spaceborne imaging spectrometer, *Remote Sensing of Environment*, 265, 112671, doi.org/10.1016/j.rse.2021.112671.

Hasenkamp, O., Lorente, A., Hu, H., Butz, A., de Brugh, J. A., and J. Landgraf, (2022), Algorithm Theoretical Baseline Document for Sentinel-5 Precursor Methane Retrieval, SRON document number SRON-S5P-LEV2-RP-001.

Irakulis-Loitxate, I., Guanter, L., Maasakkers, J., Zavala-Araiza, D., and I. Aben, (2022a), Satellites detect abatable super-emissions in one of the world's largest methane hotspot regions, *Environ. Sci. Technol.,* 56, 4, 2143-2152, doi:10.1021/acs.est.1c04873.

Irakulis-Loitxate, I., Gorroño, J., Zavala-Araiza, D., and L. Guanter (2022b), Satellites detect a methane ultra-emission event from an offshore platform in the Gulf of Mexico, *Environ. Sci. Technol. Lett.,* 9, 6, 520-524, doi:10.1021/acs.estlett.2c00225.

Jacob, D. J., Varon, D. J., Cusworth, D. H., Dennison, P. E., Frankenberg, C., Gautam, R., Guanter, L., Kelley, J., McKeever, J., Ott, L. E., Poulter, B., Qu, Z., Thorpe, A. K., Worden, J. R., and Duren, R. M., (2022), Quantifying methane emissions from the global scale down to point sources using satellite observations of atmospheric methane, *Atmos. Chem. Phys.*, 22, 9617–9646, doi.org/10.5194/acp-22-9617-2022.

Jacob, D. J., Turner, A. J., Maasakkers, J. D., Sheng, J., Sun, K., Liu, X., Chance, K., Aben, I., McKeever, J., and Frankenberg, C., (2016), Satellite observations of atmospheric methane and their value for quantifying methane emissions, *Atmos. Chem. Phys.*, 16, 14371–14396, doi.org/10.5194/acp-16-14371-2016.

de Jong, T. A., Maasakkers, J. D., Irakulis-Loitxate, I., Randles, C. A., Tol, P., and I. Aben, (2024), Daily global methane super-emitter detection and source identification with sub-daily tracking [preprint], *Earth ArXiv*, doi:10.31223/X51M52.

Lauvaux, T., Giron, C., Mazzolini, M., D'Aspremont, A., Duren, R., Cusworth, D. H., Shindell, D., and P. Cias, (2022), *Science*, 375, 6580, 557-561, doi:10.1126/science.abj4351.

Lorente, A., Borsdorff, T., Butz, A., Hasekamp, O., aan de Brugh, J., Schneider, A., Wu, L., Hase, F., Kivi, R., Wunch, D., Pollard, D. F., Shiomi, K., Deutscher, N. M., Velazco, V. A., Roehl, C. M., Wennberg, P. O., Warneke, T., and Landgraf, J., (2021), Methane retrieved from TROPOMI: improvement of the data product and validation of the first 2 years of measurements, *Atmos. Meas. Tech.*, 14, 665–684, doi.org/10.5194/amt-14-665-2021.

Maasakkers, J. D., Varon, D. J., Elfasdóttir, A., McKeever, J., Jervis, D., Mahapatra, G., Pandey, S., Lorente, A., Borsdorff, T., Foorthuis, L., R., Schuit, B. J., Tol, P., van Kempen, T., A., van Hees, R., and I. Aben, (2022), Using satellites to uncover large methane emissions from landfills, *Science Advances*, 8, 32, doi:10.1126/sciadv.abn9683.

Omara, M., Zavala-Araiza, D., Lyon, D.R., Hmiel, B., Roberts, K. A., and S. P. Hamburg, (2022), Methane emissions from US low production oil and natural gas well sites, *Nat Commun,* 13, 2085, doi.org/10.1038/s41467-022-29709-3.

Pandey, S., van Nistelrooij, M., Maasakkers, Pratik Sutar, J. D., Houweling, S., Varon, D. J., Tol, P., Gains, D., Worden, J., and I. Aben, (2023), Daily detection and quantification of methane leaks using Sentinel-3: a tiered satellite observation approach with Sentinel-2 and Sentinel-5P, *Remote Sensing of Environment*, 296, 113716, doi.org/10.1016/j.rse.2023.113716

Pedregosa, F., Varoquax, G., Gramfort, A., Thirion, M. B., Grisel, O., Blondel, M., Kobe, N., Prettenhofer, P., Weiss, R., Dubourg, V., Vanderplas, J., Passos, A., Cournapeau, D., Brucher, M., Perrot, M., Duchesnay, E. (2018), Scikit-learn: Machine Learning in Python, arXiv:1201.049v4.

Roger, J., Guanter, L., Gorroño, J., and Irakulis-Loitxate, I., (2024a), Exploiting the entire near-infrared spectral range to improve the detection of methane plumes with high-resolution imaging spectrometers, *Atmos. Meas. Tech.*, 17, 1333–1346, doi.org/10.5194/amt-17-1333-2024.

Roger, J., Irakulis-Loitxate, I., Valverde, A., Gorroño, J., Chabrillat, S., Brell., M., and L. Guanter, (2024b), High-Resolution Methane Mapping With the EnMAP Satellite Imaging Spectroscopy Mission, *IEEE Transactions on Geoscience and Remote Sensing*, 62, 1-12, doi:10.1109/TGRS.2024.3352403.

Růžička, V., Mateo-García, G., Irakulis-Loitxate, I., Johnson, J. E., Montesino San Martín, M., Allen, A., Guanter, L., & Thompson, D. R. (2025). Operational machine learning for remote spectroscopic detection of CH_4 point sources. arXiv. https://doi.org/10.48550/arXiv.2511.07719

Schuit, B. J., Maasakkers, J. D., Bijl, P., Mahapatra, G., van den Berg, A.-W., Pandey, S., Lorente, A., Borsdorff, T., Houweling, S., Varon, D. J., McKeever, J., Jervis, D., Girard, M., Irakulis-Loitxate, I., Gorroño, J., Guanter, L., Cusworth, D. H., and Aben, I., (2023), Automated detection and monitoring of methane super-emitters using satellite data, *Atmos. Chem. Phys.*, 23, 9071–9098, doi.org/10.5194/acp-23-9071-2023.

Sherwin, E.D., Rutherford, J.S., Chen, Y., Aminfard, S., Kort, E. A., Jackson, R. B., and A. R. Brandt (2023a), Single-blind validation of space-based point-source detection and quantification of onshore methane emissions, *Sci Rep,* 13, 3836, doi:10.1038/s41598-023-30761-2.

Sherwin, E. D., El Abbadi, S. H., Burdeau, P. M., Zhang, Z., Chen, Z., Rutherford, J. S., Chen, Y., and Brandt, A. R. (2024), Single-blind test of nine methane-sensing satellite systems from three continents, *Atmos. Meas. Tech*., 17, 765–782, doi.org/10.5194/amt-17-765-2024.

Stein, A. F., Draxler, R. R., Rolph, G. D., Stunder, B. J., B., Cohen, M. D., and F. Ngan (2015), NOAA's Hysplit Atmospheric Transport and Dispersion Modeling, *Bulletin of the American Meteorological Society,* 96, 12, doi:10.1175/BAMS-D-14/00110.1.

Varon, D. J., Jervis, D., McKeever, J., Spence, I., Gains, D., and Jacob, D. J., (2021), High-frequency monitoring of anomalous methane point sources with multispectral Sentinel-2 satellite observations, *Atmos. Meas. Tech*., 14, 2771–2785, doi.org/10.5194/amt-14-2771-2021.

Varon, D. J., Jacob, D. J., McKeever, J., Jervis, D., Durak, B. O., Xia, Y., and Huang Y., (2018), Quantifying methane point sources from fine-scale satellite observations of atmospheric methane plumes, *Atmos. Meas. Tech*., 11, 5673-5686, doi:10.5194/amt-11-5673-2018.

Watine-Guiu, M., Varon, D.J., Irakulis-Loitxate, I., Balasus, N., and D. J. Jacob (2023), Geostationary satellite observations of extreme and transient methane emissions from oil and gas infrastructure, *Proceedings of the National Academy of Sciences*, 120, 52, doi:10.1073/pnas.2310797120.

Appendix A: TROPOMI Hotspots

UNEP IMEO takes a 'tip-and-cue' approach through MARS where regions of interest (ROI) are identified by, for example, global mapping satellites like Sentinel-5P/TROPOMI or GOSAT. ROIs are then further explored using high-resolution satellite imagery to attribute individual methane plumes to the facility-scale, either through manual inspection of imagery or using machine learning models (see Appendix E).

Through partnership with the Netherlands Institute for Space Research (SRON), on a 3-weekly basis UNEP IMEO receives 'hot spots' from Sentinel-5P/TROPOMI, that indicate regions of semi-persistent elevated methane concentration associated with one or more individual sources. Here we describe, briefly, the procedure for calculating 'hot spots' used for determining ROIs in MARS. More details are found in Maassakers *et al.* (2022).

SRON uses the TROPOMI XCH4 data described by Lorente *et al.*, (2021) and applies a wind-rotation technique to the long-term averaged methane data. XCH4 data is further albedo-bias corrected over land and filtered such that methane precision is < 10 ppb, VIIRS cloud fraction is < 0.02, SWIR aerosol optical depth < 0.13, and SWIR albedo is > 0.02. Following Zhu *et al.* (2017), TROPOMI data is first oversampled to identify regions of methane enhancement, Then, based on the 10-m ERA5 reanalysis winds, XCH4 data is rotated such that the wind vector is always oriented to the north. This allows SRON to determine the most likely region of methane sources when downwind concentrations are consistently enhanced compared to the upwind in the rotated, oversampled average data. Visual imagery or emission databases are also used to manually determine the most likely emission source associated with the wind-rotated, averaged TROPOMI XCH4 observations.

Appendix B: Sentinel-5P/TROPOMI Plume Detection, Quantification, and Uncertainty Analysis

Sentinel-5P/TROPOMI data are provided to UNEP IMEO by Copernicus Atmosphere Monitoring Service (CAMS) and processed by SRON following Schuit et al., (2023). Here we briefly summarize the process from that work. First, bias corrected CH4 data (S5P L2 CH4) is downloaded from the European Space Agency (ESA) via the Copernicus Data Space Ecosystem. Processing of plumes is done only on data with Level 2 data quality value (qa_value) > 0.4, methane precision < 10 ppb, SWIR aerosol optical depth <0.13, near-infrared (NIR) aerosol optical depth fraction <0.02. Images are destriped using the approach described in Borsdorff et al., (2018).

Next, the plume-like structures are detected on the TROPOMI dry-air mixing ratios using a convolutional neural network (CNN) made of two convolutional blocks and two fully connected layers. The CNN is followed by a support vector machine (SVM) to separate plumes from retrieval artefacts with additional information and engineered features. The models were trained using verified methane plumes from 2018-2020 captured by TROPOMI.

The methane enhancement is calculated by subtracting the total methane column mass by the background levels. The local background value is computed as the median value of the pixels outside the plume mask in the scene. Then, the quantification of the fluxrate uses the integrated mass enhancement (IME) method (see Appendix G) with calibrated windspeeds from ERA5 10m winds (Hersbach et al., 2020), GEOS FP 10m winds, and GEOS FP planetary boundary layer (PBL) winds (Molod et al., 2012). Winds are converted into effective windspeeds using linear relationships with slopes and intercepts detailed in Table A.1. The mean of the three windspeeds is then used to calculate emission fluxrates.

WIND	A	B
ERA5 – 10M	0.59	0.00
GEOS FP – 10M	0.59	0.00
GEOS FP - PBL	0.47	0.31

Table A.1: Coefficients for linear relationship between u_{eff} and u as in Equation A.6.

The uncertainty in the fluxrate is the standard deviation of the ensemble of results obtained by varying the different parameters involved in the quantification. The parameters include the threshold for plume masking (1.3-2.3 standard deviations), the calculation of the background concentration (±2 times the mean), wind speed values (±50%), and the effective windspeed coefficients (±5%).

Appendix C: Matched-Filter (MF) Retrieval Method

The Matched-Filter (MF) image processing technique is a data-driven method applied to images from hyperspectral instruments in spectral fitting windows specific to methane (e.g., 2110 to 2450-nm). Data-driven methods such as MF constrain the retrieval of per-pixel methane enhancement relative to the background using statistics derived from the image. An advantage of this approach is that this methodology can account for radiometric and spectral errors typical of satellite imaging spectroscopy data and are computationally efficient (Guanter *et al.*, 2021). The MF takes the form:

$$XCH4 = \frac{(\boldsymbol{L}-\boldsymbol{m})^T \sum^{-1} \boldsymbol{t}}{\boldsymbol{t}^T \sum^{-1} \boldsymbol{t}}$$ **(Equation A.1)**

Where *L* is the analyzed per-pixel spectrum, μ is the mean of the background radiance, Σ is the covariance of the background radiance, and *t* is the target spectrum that represents the perturbation of the background radiance signal by a methane enhancement [W m^{-2} sr^{-1} ppm^{-1}]

Following Guanter *et al.*, 2021, the premise of the MF methodology is that each observed spectrum can be decomposed into a mean spectrum plus a perturbation spectrum, which is due to changes in the methane column concentration. A unit-absorption spectrum (K_{CH4}) is first generated using radiative transfer simulations (e.g., MODTRAN; Berk *et al.*, 2014) to represent a change in radiance for 1 ppm increase in CH_4 concentration over a 1 m pathlength. Beer-Lambert's Law shows that the total radiance spectrum can be decomposed into a spectrum with no methane absorption (L_{BKG}) and XCH4 using the CH4 unit absorption spectrum K_{CH4} (Roger *et al.*, 2024):

$$L_{total} = L_{bkg} e^{(XCH4 \cdot K_{CH4})}$$ **(Equation A.2)**

Assuming a column-height of 8-km, Equation A.2 can be linearized for the matched-filter method such that Equation A.1 is derived from the Beer-Lambert's Law.

The MF algorithm also uses per-pixel column basis statistics (mean spectrum and covariances) to account for the across-track radiometric- and spectral-instrument response typical of imaging spectrometers. Running an MF retrieval over all pixels of an image produces XCH4 maps with a sampling commensurate with instrument pixel size (e.g., 30 m for PRISMA). UNEP IMEO is currently using the latest MF codebase version developed by the Universitat Politèchnica de València (UPV) following Roger *et al.*, (2024) which computes both the standard MF and the wide-window matched filter (WWMF). The WWMF approach utilizes a broader spectral window to better constrain the background, which attenuates or removes retrieval artifacts while also reducing background noise.

Appendix D: Multi-Band Multi-Pass (MBMP) Retrieval Method

While hyperspectral instruments scan the Earth over broad spectral bands (e.g., 200-4000 nm) with high spectral resolution (e.g., 1-10 nm spectral line spacing), multi-spectral instruments view discreet, broad spectral bands, generally over smaller portions of the spectrum. For example, Sentinel-2 and Landsat-8/9 have 13 and 7 broad spectral bands, respectively, from the visible to the shortwave infrared (SWIR). To retrieve methane with these instruments with lower-spectral resolution, methane vertical column concentration can be derived either by comparing a single spectral band with and without a methane plume, or by comparing adjacent bands, one sensitive to methane one not, but with similar response to the surface and aerosol (Varon *et al.*, 2021). UNEP uses the latter approach, using channels B12 (central wavelength 2190 nm, 189 nm bandwidth) and B11 (central wavelength 1610 nm, 90 nm bandwidth) for Sentinel-2 and channels B7 (2.11 – 2.29 μm) and B6 (1.57-1.65 μm) for Landsat 8/9, where channels B12 and B7 are the methane-sensitive channels. For GOES, UNEP IMEO follows Watine-Guiu *et al.*, (2023) using channels B5 (1.6 μm) and B6 (2.2 μm), the latter being the methane-sensitive channel.

UNEP IMEO uses the MBMP method developed by Gorroño *et al.*, (2023) with a clear-sky reference image for each location (ref in equation below). The reference image is selected across other images over the same location that the scene under consideration (denoted by plume in the equation), the retrieval is given by:

$$MBMP = \frac{c\frac{\rho_{2.3\mu m\, plume}}{\rho_{1.6\mu m\, plume}}}{c'\frac{\rho_{2.3\mu m\, ref}}{\rho_{1.6\mu m\, ref}}} \quad \textbf{(Equation A.3)}$$

where $\rho_{2.3\mu m}$ corresponds to the reflectance in methane sensitive band and,$_{1.6\mu m}$ to the reflectance of the reference band. The coefficients *c and* c' are calculated as the inverse of the average of the $\rho_{2.3\mu m}/\rho_{1.6\mu m}$ ratio (c for the scene under consideration and c' for the reference image). The MBMP is an estimation of the transmittance of the $\rho_{2.3\mu m}/\rho_{1.6\mu m}$ ratio; to obtain the per-pixel methane enhancement (XCH_4) we use a look-up table (LUT) generated with MODTRAN that contains the simulated transmittance of $\rho_{2.3\mu m}/\rho_{1.6\mu m}$ for different XCH_4 concentrations and viewing geometries. This methodology has been validated in the work of Gorroño *et al.*, (2023) with simulated plumes and in the single-blind controlled release studies of *Sherwin et al., 2024*, *2023*.

For Sentinel-2 and Landsat, radiance values are filtered out for clouds and their shadows following Aybar et al., (2022).

Appendix E: UNEP MARS-S2L model

UNEP IMEO has developed MARS-S2L, the first large-scale operational machine learning model for detecting methane emissions in multispectral (Sentinel-2 and Landsat) satellite imagery (Allen et al., 2025). The model is based on a UNet architecture that takes 16 input channels, including 6 multispectral bands from current and reference passes, cloud masks (CloudSEN12, Aybar et al., (2022)), ERA5 wind vectors, and MBMP differencing. To handle class imbalance, training utilizes a physics-based plume simulation scheme based on the simulation methodology of Gorroño *et al.,* (2023).

MARS-S2L substantially outperforms previous baselines (such as MBMP thresholding and earlier models like CH4Net, Vaughan et al., (2024)), achieving 78% recall with an 8% false positive rate at previously unseen sites. The minimum detection limit is approximately 2.5 t/h (90% probability of detection) for Sentinel-2.

In practice, UNEP IMEO uses MARS-S2L to continuously monitor data from Sentinel-2 and Landsat-8/9 globally. The model outputs a pixel-wise prediction of the probability of a pixel being part of a methane plume, which is then used to flag plume candidates for human validation. This AI-assisted workflow has enabled the discovery of new sites and the successful mitigation of persistent emitters worldwide.

Appendix F: UNEP MARS-HSI model

UNEP IMEO has also deployed an operational machine learning system for detecting methane plumes in hyperspectral satellite data, including EMIT, PRISMA, and EnMAP (Růžička *et al.,* 2025). The MARS-HSI model utilizes a UNet architecture with a MobileNetV3 encoder (~6.69M parameters). Instead of raw radiance, the model takes as input the Wide-Window Matched-Filter (WWMF) retrieval and the RGB reflectance image. The system was trained on a diverse global dataset of annotated hyperspectral methane plumes, which were rigorously double-validated by expert analysts.

A key technical contribution of the MARS-HSI system is the use of model ensembling, which reduces false positive detections by over 74% compared to prior state-of-the-art methods such as STARCOP (Ruzicka et al 2023). Furthermore, the model demonstrates strong zero-shot cross-sensor generalization—models trained exclusively on EMIT data perform effectively on PRISMA and EnMAP imagery, with performance further enhanced through sensor-specific fine-tuning.

In practice, MARS-HSI is used to process incoming hyperspectral data globally. The model generates pixel-wise predictions to flag candidate methane plumes, which are subsequently reviewed by human analysts for final validation. This AI-assisted pipeline significantly accelerates the analysis of large hyperspectral data volumes and has directly contributed to verified mitigation actions worldwide

Appendix G: Plume masking and attribution

UNEP IMEO uses a semi-automated approach to plume masking for high-resolution imagers. For multispectral imagers (Sentinel-2, Landsat), MARS automatically downloads the data, retrieves XCH4 using the MBMP approach, and runs the MARS-S2L AI model (see Appendix E; Allen et al., 2025) to detect and mask the plume. For hyperspectral imagers (EMIT, PRISMA, EnMAP), data is ingested automatically, XCH4 is retrieved using both the MF and WWMF approaches, and pre-processed using the MARS-HSI AI model (see Appendix F; Růžička et al., 2025). While EnMAP and PRISMA are sometimes tasked, all data is automatically ingested and processed in the same manner.

Detected plumes generate an alert within the MARS PlumeViewer application, an internal analysis environment designed to streamline review, attribution, and automated report generation. Within PlumeViewer, analysts have access to a comprehensive suite of contextual data, including multiple methane retrieval methodologies (e.g., MBMP, MF, WWMF) overlayed to verify a consistent signal, high-resolution RGB imagery, shortwave infrared (SWIR) bands, cloud masks, and wind vectors. To ensure high confidence in the published data, MARS employs a rigorous double-round human validation protocol. A first remote sensing expert reviews AI-flagged candidates, visually inspecting the image to discard false positives and manually redrawing the plume using the AI mask as a suggestion. Importantly, not all plumes are flagged by AI models (Allen *et al.*, 2025; Růžička *et al.*, 2025); analysts also manually discover and flag additional plumes while browsing the imagery in PlumeViewer. Plumes are validated using multiple signals to verify coherence, wind alignment, RGB correlation, flare signal, marginal cloud presence, and reference scan corruption. The spatial scope of this analysis depends on the sensor: multispectral analysis (Sentinel-2, Landsat) is typically restricted to a 2 km × 2 km region around known monitoring locations, whereas hyperspectral processing (EMIT, PRISMA, EnMAP) evaluates the full satellite tile, enabling broader discovery of new emission sources. Once validated, the detection is reviewed by a second expert for final confirmation before any stakeholder notification is issued, and the plume is published in the Eye on Methane data platform.

Following validation, the confirmed plumes undergo an attribution process to identify the responsible operators and owners. This is achieved by linking the emission location to facility-level infrastructure datasets, such as the Oil and Gas Infrastructure Mapping (OGIM) database and Rystad Energy. PlumeViewer facilitates this semi-automated attribution workflow by overlaying the validated plume footprints with these external databases, allowing analysts to classify sources by sector, subsector, source type, basin, and operator. This end-to-end workflow—from AI detection to double-validated attribution—enables MARS to generate actionable, source-level notifications for governments and companies.

Appendix H: Plume emission quantification and uncertainty methodology

UNEP IMEO uses the Integrated Mass Enhancement Method (IME) as detailed in Varon *et al.* (2021) for plume emission rate quantification (*Q*; mass methane per time units):

$$Q = \frac{IME \times U_{eff}}{L}$$ **(Equation A.4)**

where the IME is computed as the sum of the column enhancements over the binary plume mask that separates the plume from the background:

$$\frac{IME}{A} = \sum_{j=1}^{N} XCH4_j$$ for *N* pixels **(Equation A.5)**

and *L* is the square root of the area of the plume mask (*L = sqrt(A)*), and the effective wind speed u_{eff} is a function of the 10-m wind speed u_{10m} from reanalysis data (e.g. ERA5 wind or NASA GEOS-FP):

$$u_{eff} = a \times u_{10m} + b$$ **(Equation A.6)**

Coefficients *a* and *b* in Equation A.6 depend on the satellite in question according to Table A.2 below:

SATELLITE	A	B

LANDSAT-8/9	0.33	0.45
SENTINEL-2	0.33	0.45
PRISMA	0.34	0.44
ENMAP	0.34	0.44
EMIT	0.36	0.66
GOES	-	-

Table A.2: Coefficients for logarithmic relationship between u_{eff} and u_{10m} in Equation A.6.

For all plume quantifications, UNEP IMEO provides an emissions uncertainty estimate. First, except for GOES, we calculate the uncertainty in the *IME* as function of instrument-specific uncertainty in methane enhancement retrieval in ppm•m (*e.g.,* Jacob *et. al.,* 2022). An assumed error of 50% in u_{10} is then propagated with Monte Carlo techniques to u_{eff}, and finally errors in both *IME* and u_{eff} are propagated to *Q* again using a Monte Carlo technique. Note that the instrument-specific uncertainty in the enhancement is used to calculate the *IME* error is determined for specific viewing conditions (e.g., generally over a bright, homogeneous surface with clear skies). While it is expected that this uncertainty will vary with surface reflectance and scene complexity, it is too computationally burdensome to calculate this quantity for all possible scenes.

To ensure physical consistency and robustness across sensors, the quantification methodology includes specific handling for enhancements and plume extents. First, negative methane enhancement values are allowed to contribute to the integrated enhancement (IME) rather than being clipped to zero, which avoids introducing a positive bias. If the total integrated enhancement is negative, the flux rate is reported as zero. Second, for very large plume extents, the integration region is cropped to a 3 km radius around the source before computing the IME. This keeps the quantification within the spatial regime where the IME assumptions and effective-wind calibrations are most applicable.

GOES quantification and uncertainty analysis follows Watine-Guiu *et al.* (2023).
On February 20, 2026, UNEP IMEO completed a comprehensive requantification of all historical plumes detected by Sentinel-2, Landsat-8/9, EMIT, PRISMA, and EnMAP to harmonize quantification behavior and apply updated effective wind speed calibrations (see below). The most significant impact was observed in EMIT detections, which showed a systematic reduction (mean relative bias

of approximately -40%) due to an updated effective wind calibration derived from large-eddy simulations. For the other satellites, the changes were modest and primarily addressed edge cases. As part of this effort, all outlier plumes (those with flux rates < 300 kg/h or > 50 t/h) underwent an additional manual review to ensure the highest data quality.

The new effective windspeed coefficients for EMIT result from the analysis of simulated plumes, a methodology proven with other satellites like EnMAP (Roger et al., 2024). EDF researchers performed an in-house analysis generating 80,000 synthetic methane retrievals of EMIT. The retrievals resulted from adding multiple levels of instrument noise (150-300 ppb) to snapshots of simulated plumes under various wind speeds (~1-6 m s^{-1}), wind directions (0-180º) and emission rates (0.05-21 t h^{-1}). The simulated plumes were the same as those in Varon et al., (2021).

A simple detection algorithm processed the retrievals and produced a plume mask. The mask is used to calculate the Integrated Mass Enhancement (IME) and the length of the plume ($L = \sqrt{A}$, where A is the mask area). The detection algorithm included (1) a low pass filter to remove outliers, (2) thresholding at twice the noise standard deviation, and (3) a screening of blobs with areas larger than 5-12 pixels.

The effective wind speed U_{eff} was derived from Equation A.7. The simulation provides the flux rate Q, while the detection pipeline provides IME and L:

$$Q = \frac{U_{eff} IME}{L} \rightarrow U_{eff} = \frac{QL}{IME}$$ **(Equation A.7)**

A linear regression between U_{eff} and the simulated 10-m wind speed (U_{10}) (Figure A.1) gives the calibration coefficients shown in Table A.2.

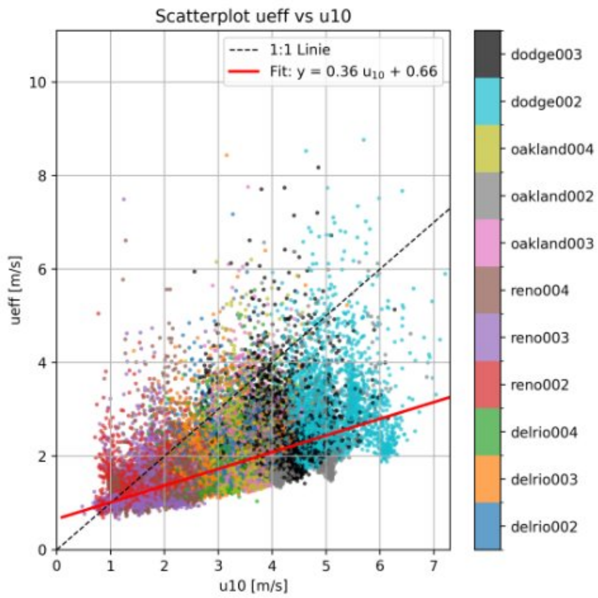

Fig. A.1: Calibration of the effective windspeed for EMIT. On the left, the red line is the regression between the 10-m wind speed used in the simulation (x axis) and the effective wind speed calculated as in Equation A.7.

Appendix I: Data Provenance

Here we detail the raw satellite data, download frequency, and data repository location for all high-resolution satellite data used by UNEP IMEO in Table A.3. In Table A.4 we also provide any of the ancillary data we use in the computation of plume masks or flux rates.

SATELLITE	PROCESSING LEVEL	DOWNLOAD FREQUENCY	DATA REPOSITORY LOCATION
SENTINEL-2	Harmonized Sentinel-2 L1C	Daily	Google Earth Engine
LANDSAT-8/9	Tier 1 Calibrated TOA reflectance	Daily	Google Earth Engine Landsat 9 and Landsat8
PRISMA	L1B	Daily (and on Demand tasking)	ASI
ENMAP	L1B	Daily (and on demand tasking)	DLR
GOES	L1B	On Demand	AWS (via NOAA)

EMIT	L1B and L2BCH4ENH (latter, when available)	Daily	NASA EarthData

Table A.3: Data Provenance of Methane-Detecting Satellite Imagery

DATA NAME	DATA NAME	DOWNLOAD FREQUENCY	DATA REPOSITORY
ERA5 WINDS	ERA5-Land Hourly	On Demand	Google Earth Engine
NASA GEOS FP WINDS	GEOS0-FP 1-hour time averaged wind	On Demand	NADA NCCS
JPL XCH4 PRODUCTS	L2B Methane Enhancement	When Available	NASA Earthdata
TROPOMI HOTSPOTS	L4	Every 3-weeks	Provided by email from SRON
CAMS/ECMWF/SRON S5P PLUMES	L4	Daily	CAMS Methane Explorer portal
SENTINEL-3/NOAA-VIIRS PLUMES	L4	When Available	Provided by email from SRON
CARBON MAPPER	L4	When Available	Provided by API from CarbonMapper

Table A.4: Ancillary Data Provenance

Appendix J: Persistency calculation method

Persistency (P) is estimated as the ratio between the number of detections (D) and the number of valid overpasses (M) (*Ayasse et al., 2024*):

$$\hat{P} = D/M \quad \textbf{(Equation A.8)}$$

The value of M is the sum of the number of detections (D) and non-detections (N_q) with sufficient quality to measure the event. N_q excludes observations limiting the retrieval (clouds, haze, aerosols, shadows or smoke) and overpasses from sensors not capable of detecting the event. To determine whether the sensor can detect the event, the algorithm evaluates its Probability of Detection (PoD) on the historical detections median flux rate ($\bar{Q}$). The algorithm considers that the observation is valid If there is more than 50% chance of detecting an event like $\bar{Q}$ ($PoD(\bar{Q}) > 0.5$).

The PoD for each sensor (Figure A.2) was determined based on the frequency of detected emissions (see e.g., Ehret et al., 2022) from MARS-IMEO historical records. The frequency of detected emissions is the combination of the true frequency of emissions (usually following a power law curve) and the ability of the monitoring system to detect those events (logistic curve), i.e. the PoD. At high emission rates, the observed frequency aligns closely with the underlying distribution of emissions. At lower flux rates, limitations of the system become significant, and the frequency of detected emissions diverges from the power law. MARS-IMEO inferred the PoD by fitting simultaneously a power law and a logistic curve PoD to the frequency of detected emissions from each sensor. The PoDs in Figure A.2 are not applicable outside the context of MARS-IMEO, as they reflect the average operational conditions (e.g., wind, noise, etc.) experienced with each sensor and its working pipeline (algorithms, manual review, etc.).

Persistency is assumed to follow a Binomial distribution, with a standard error of the observed frequency given by:

$$\sigma_{\hat{P}} = \sqrt{\frac{\hat{P}(1-\hat{P})}{M}} \quad \textbf{(Equation A.9)}$$

Where $\hat{P}$ is the estimate of the persistency and M is the number of valid observations.

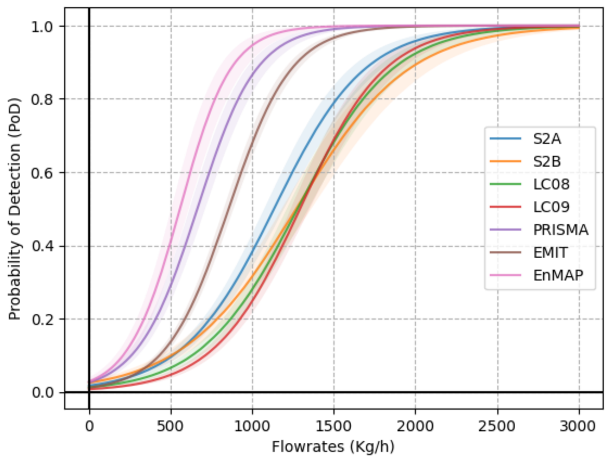

Fig. A.2: Probability of Detection for the most frequent satellites and sensors used by MARS for methane detection and quantification. Abbreviations: S2A – Sentinel-2A, S2B – Sentinel-2B, LC08 – Landsat-8, LC09 – Landsat-9.